

Increasing Isotropy of Intrinsic Compliance in Robot Arms through Biarticular Structure^{*}

Valerio Salvucci^{*} Travis Baratcart^{*} Takafumi Koseki^{*}

^{*} *Department of Electrical Engineering and Information System,
The University of Tokyo, 3-7-1 Hongo, Bunkyo, Tokyo, 113-8656, Japan
(e-mail: valerio@koseki.t.u-tokyo.ac.jp, b_travis@koseki.t.u-tokyo.ac.jp,
takafumikoseki@ieee.org).*

Abstract: In human-robot interaction passive compliance is fundamental for safety, however stiffness is necessary for performance. These two factors motivate intrinsic compliance modulation in robots interacting with humans. Variable Stiffness Actuators (VSAs) allow for simultaneous position and stiffness control of a joint, therefore they have been implemented in the realization of intrinsically compliant and high performance robot arms. Most applications employ VSAs in a monoarticular structure, that is one actuator produces torque about one joint. In the biological world however, bi-articular muscles (muscles spanning two joints) play a fundamental role in motion control for humans, not only reducing link inertia, but also increasing isotropy of end effector force and compliance. In this work, a robot arm with VSAs and two interchangeable actuation structures (the traditional monoarticular and human-like biarticular) is built. The end effector intrinsic compliance in both the actuation structures is measured. Experimental results suggest that the biarticular VSA structure is more suitable for compliant robot arms.

Keywords: Mechatronic systems, Motion control systems, Robots manipulators

1. INTRODUCTION

In human-robot interaction, as well for robots operating in presence of humans, passive compliance is fundamental to guarantee safety Bicchi et al. (2001). A widely known approach to achieve passive compliance is through the use of elastic elements between the actuator and the joint, namely Series Elastic Actuators (SEAs) Pratt and Williamson (1995). A limit of SEAs is that the compliance can not be varied without the use of feedback control as compliance depends on the mechanical characteristic of the elastic elements, which is constant English and Russell (1999). In order to overcome the bandwidth limitations of feedback control, while at the same time allowing for passive compliance regulation, Variable Stiffness Actuators (VSAs) are rising in interest. VSAs allow for simultaneous position and stiffness control of a joint, and are therefore employed in intrinsically compliant manipulators Ham et al. (2009), Koganezawa et al. (2006), Migliore et al. (2005), Hurst et al. (2010), Ham et al. (2007), Wolf and Hirzinger (2008), Tsagarakis et al. (2009), Chalon et al. (2010), Palli et al. (2007). In most of these robot arms, the VSAs are implemented in a monoarticular structure (i.e. a VSA produces torque about a single joint).

Unlike conventional robot arms with monoarticular actuation, humans and animals incorporates bi-articular muscles — muscles spanning two consecutive joints — to regulate stiffness stabilizing unstable dynamics (for example running over rough terrain Daley et al. (2006)), to increase accuracy of movements Smeets (1994), and to transfer power from proximal to distal

joints Van Ingen Schenau (1989). For these reasons interest in robots with bi-articular actuators has been rising. Implementation of biarticular actuation in robotic applications has shown numerous advantages. Biarticular actuators dramatically increase the range of end effector impedance which can be achieved without feedback Hogan (1985), increase the capability of path tracking and disturbance rejection Salvucci et al. (2011c), Horita et al. (2002), allow for precise output force control Salvucci et al. (2013b), improve balance control for legged robots without force sensors Oh et al. (2010). and increase isotropy of maximum end effector force Salvucci et al. (2013a), Salvucci et al. (2013c). However, the combination of VSAs and biarticular structure is a new approach which has not yet been deeply investigated.

In this work, a robot arm with VSAs and two interchangeable actuation structures — the traditional monoarticular and human-like biarticular — is built. The end effector compliance in both the actuation structures is measured.

The paper is organized as follows. Modeling of bi-articularly actuated robot arms is shown in section 2. In section 3 the variable stiffness mono- and bi-articular actuator structures are illustrated. In section 4, the two-link planar robot arm with VSAs is described together with the experimental setup. The results are shown and analyzed in section 5. Finally, this work is concluded in section 6.

2. MODELING BI-ARTICULAR ACTUATION IN ROBOT ARMS

Animal and human limbs present a complex musculoskeletal structure based on mono- and multi- articular muscles:

- (1) Mono-articular muscles produce torque about one joint.

^{*} The authors would like to thank Japanese Society for the Promotion of Science (JSPS). This work was supported by JSPS KAKENHI Grant NUMBER 24.02748.

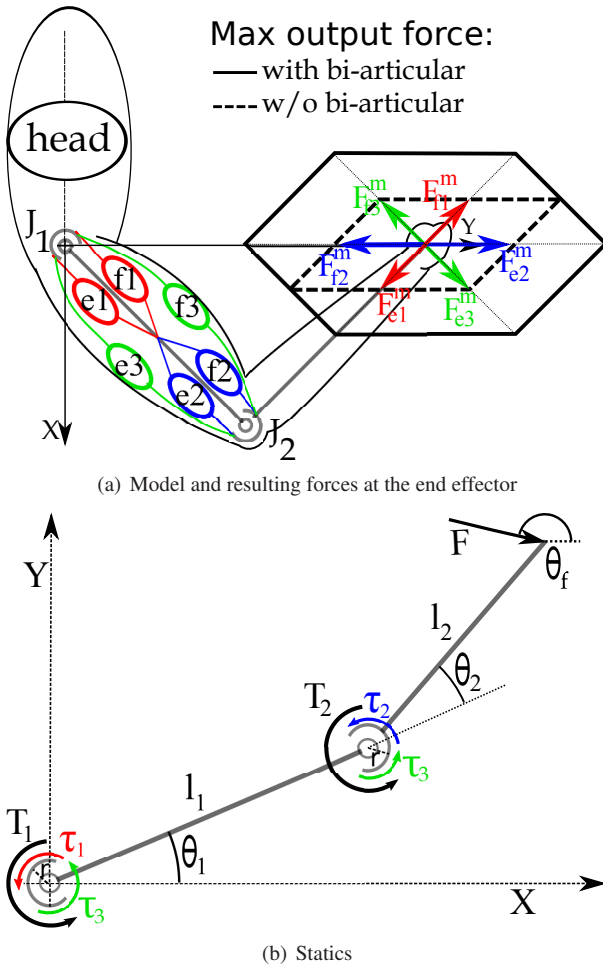


Fig. 1. Two-link arm with four mono- and two bi-articular actuators

(2) Multi-articular muscles produce torque about more than one joint.

A widely used simplified model of the complex animal musculoskeletal system Fukusho et al. (2010), Kumamoto et al. (1994), Oh et al. (2011), Salvucci et al. (2011a), Salvucci et al. (2011b) with the maximum end effector forces at the end effector is shown in Fig. 1(a). This model is based on six contractile actuators — three extensors (e1, e2, and e3) and three flexors (f1, f2, and f3) — coupled in three antagonistic pairs:

- e1–f1 and e2–f2: couples of mono-articular actuators that produce torques about joint 1 and 2, respectively.
- e3–f3: couple of bi-articular actuators that produce torque about joint 1 and 2 simultaneously.

The six actuators produce contractile forces e_i or f_i for $i = (1, 2, 3)$ with respective maximum value e_i^m or f_i^m . The resulting end effector forces are F_{ei} and F_{fi} for $i = (1, 2, 3)$ with respective maximum values F_{ei}^m and F_{fi}^m .

The resulting statics are shown in Fig. 1(b) where \mathbf{F} is a general force at the end effector; $\mathbf{T} = [T_1, T_2]^T$ are total torques about joints 1 and 2, respectively; $\boldsymbol{\tau}$ represents the actuators torques: τ_1 and τ_2 are torques produced by mono-articular actuators about joints 1 and 2, respectively, while τ_3 is the bi-articular torque produced about both joints simultaneously. The resulting joint torques are Salvucci et al. (2013a):

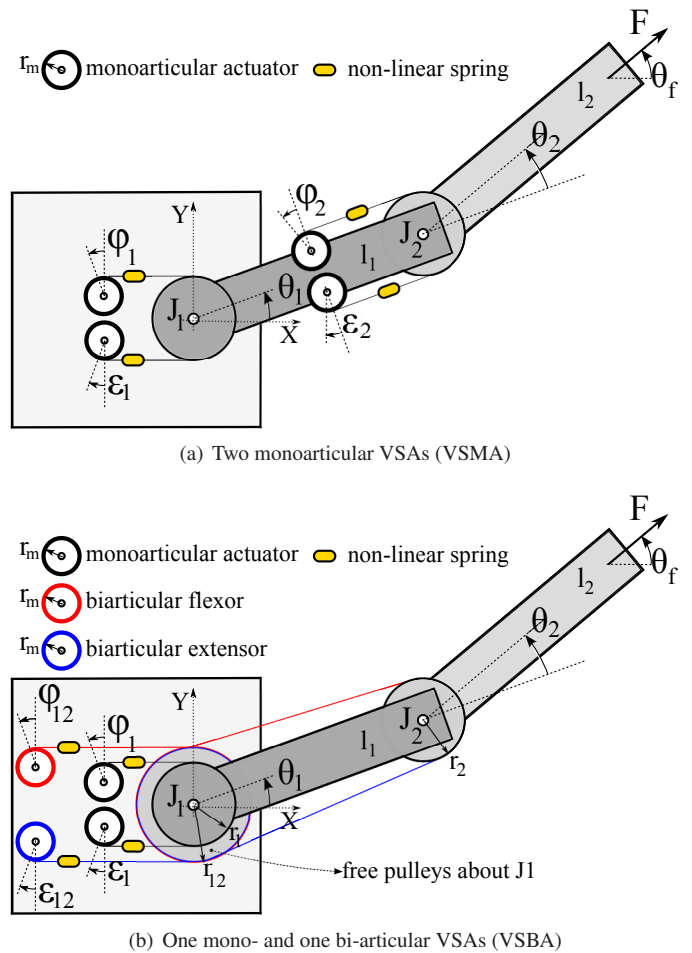


Fig. 2. Two-link intrinsically compliant manipulators: mono-articular VSAs (VSMA) and bi-articular VSAs (VSBA) structures

$$\mathbf{T} = \mathbf{B}\boldsymbol{\tau} = \begin{bmatrix} 1 & 0 & 1 \\ 0 & 1 & 1 \end{bmatrix} \begin{bmatrix} \tau_1 \\ \tau_2 \\ \tau_3 \end{bmatrix} \quad (1)$$

3. VARIABLE STIFFNESS MONO- AND BI-ARTICULAR ACTUATOR STRUCTURES

3.1 Structure

In Fig. 2 two actuation structures for a two-link intrinsically compliant robot arm are shown. The VSA are made of two antagonistic motors, each one employing a nonlinear elastic element in the transmission system. The first one in Fig. 2(a), referred as Variable Stiffness Monoarticular Actuator (VSMA) structure in the following, is the conventional one implemented in intrinsically compliant robot arm. It consists of two VSAs, each connected to one joint as a monoarticular actuator. In Fig. 2(b), referred as Variable Stiffness Biarticular Actuator (VSBA) structure in the following, consists of one VSA connected to joint 1 as a monoarticular actuator, and a VSA connected to both joints 1 and 2 as a biarticular actuator by means of a free pulley system.

3.2 Modelling

Given the reference system in Fig. 2, the spring displacements between joints and respective actuator are:

$$\Delta l_{\phi 1} = \phi_1 r_m - r_1 \theta_1 \quad (2)$$

$$\Delta l_{\varepsilon 1} = \varepsilon_1 r_m + r_1 \theta_1 \quad (3)$$

$$\Delta l_{\phi 2} = \phi_2 r_m - r_2 \theta_2 \quad (4)$$

$$\Delta l_{\varepsilon 2} = \varepsilon_2 r_m + r_2 \theta_2 \quad (5)$$

$$\Delta l_{\phi 12} = \phi_{12} r_m - r_{12} \theta_1 - r_2 \theta_2 \quad (6)$$

$$\Delta l_{\varepsilon 12} = \varepsilon_{12} r_m + r_{12} \theta_1 + r_2 \theta_2 \quad (7)$$

where $\boldsymbol{\theta} = [\theta_1, \theta_2]^T$ is the joint angle position, ϕ_i and ε_i are respectively the flexor and extensor monoarticular actuator angle displacements in radians, r_m is the radius of the motor pulleys, and r_1 and r_2 are the radii of pulleys at joint 1 and 2, respectively. ϕ_{12} and ε_{12} are respectively the flexor and extensor biarticular actuator angle displacements in radians, r_{12} is the radius of the free pulley about joint 1 through which the biarticular actuators produce torque about joint 1.

For the VSMA structure, the joint torques (\mathbf{T}^{VSMA}) are:

$$\mathbf{T}^{VSMA} = \begin{bmatrix} T_1^{VSMA} \\ T_2^{VSMA} \end{bmatrix} = \begin{bmatrix} \tau_1 \\ \tau_2 \end{bmatrix} = \begin{bmatrix} r_1(f_{\phi 1} - f_{\varepsilon 1}) \\ r_2(f_{\phi 2} - f_{\varepsilon 2}) \end{bmatrix} \quad (8)$$

where $f_{(\phi_i, \varepsilon_i)}$ for $i = (1, 2)$ are the forces produced by the springs.

The spring stiffness matrix for the VSMA structure is:

$$\mathbf{K}_s^{VSMA} = \begin{bmatrix} k_{\phi 1} & 0 & 0 & 0 \\ 0 & k_{\varepsilon 1} & 0 & 0 \\ 0 & 0 & k_{\phi 2} & 0 \\ 0 & 0 & 0 & k_{\varepsilon 2} \end{bmatrix} \quad (9)$$

The resultant joint stiffness matrix is:

$$\begin{aligned} \mathbf{K}_j^{VSMA} &= (\mathbf{J}_t^{VSMA})^T \mathbf{K}_s \mathbf{J}_t^{VSMA} \\ &= \begin{bmatrix} r_1^2(k_{\phi 1} + k_{\varepsilon 1}) & 0 \\ 0 & r_2^2(k_{\phi 2} + k_{\varepsilon 2}) \end{bmatrix} \end{aligned} \quad (10)$$

where,

$$(\mathbf{J}_t^{VSMA})^T = \begin{bmatrix} r_1 & -r_1 & 0 & 0 \\ 0 & 0 & r_2 & -r_2 \end{bmatrix} \quad (11)$$

It is important to note that in order to have an intrinsic stiffness modulation, the force-displacement relation of the spring (i.e. $k_{\phi_i}, k_{\varepsilon_i}$ for $i = (1, 2)$) has to be nonlinear English and Russell (1999).

For the VSBA structure, the resulting joint torques (\mathbf{T}^{VSBA}) are:

$$\begin{aligned} \mathbf{T}^{VSBA} &= \begin{bmatrix} T_1^{VSBA} \\ T_2^{VSBA} \end{bmatrix} = \begin{bmatrix} \tau_1 + \tau_3 \\ \tau_3 \end{bmatrix} \\ &= \begin{bmatrix} r_1(f_{\phi 1} - f_{\varepsilon 1}) + r_{12}(f_{\phi 12} - f_{\varepsilon 12}) \\ r_2(f_{\phi 12} - f_{\varepsilon 12}) \end{bmatrix} \end{aligned} \quad (12)$$

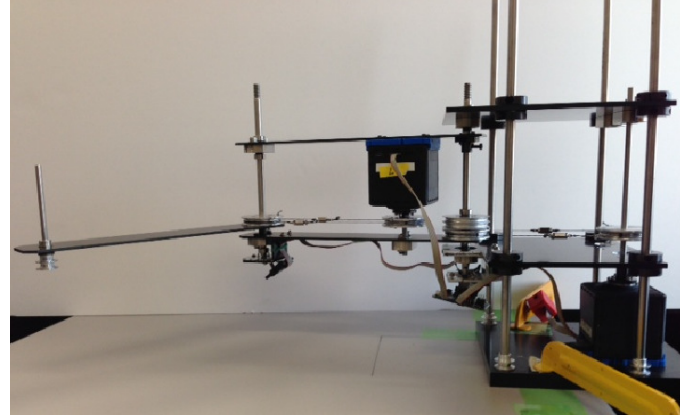
The spring stiffness matrix for the VSBA structure is:

$$\mathbf{K}_s^{VSBA} = \begin{bmatrix} k_{\phi 1} & 0 & 0 & 0 \\ 0 & k_{\varepsilon 1} & 0 & 0 \\ 0 & 0 & k_{\phi 12} & 0 \\ 0 & 0 & 0 & k_{\varepsilon 12} \end{bmatrix} \quad (13)$$

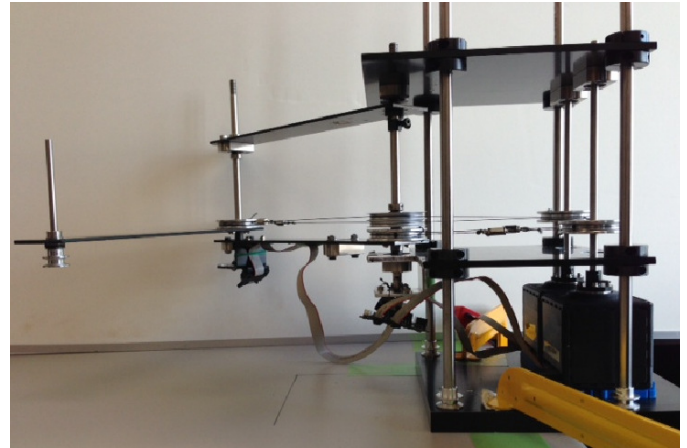
The resulting joint stiffness matrix is:

$$\begin{aligned} \mathbf{K}_j^{VSBA} &= (\mathbf{J}_t^{VSBA})^T \mathbf{K}_s \mathbf{J}_t^{VSBA} \\ &= \begin{bmatrix} r_1^2(k_{\phi 1} + k_{\varepsilon 1}) + r_{12}^2(k_{\phi 12} + k_{\varepsilon 12}) & \\ & r_2 r_{12}(k_{\phi 12} + k_{\varepsilon 12}) \\ r_2 r_{12}(k_{\phi 12} + k_{\varepsilon 12}) & \\ & r_2^2(k_{\phi 12} + k_{\varepsilon 12}) \end{bmatrix} \end{aligned} \quad (14)$$

where,



(a) VSMA



(b) VSBA

Fig. 3. Two-link planar arm in VSMA and VSBA structures

$$(\mathbf{J}_t^{VSBA})^T = \begin{bmatrix} r_1 & -r_1 & r_{12} & -r_{12} \\ 0 & 0 & r_2 & -r_2 \end{bmatrix} \quad (15)$$

The stiffness matrix in Cartesian coordinates, \mathbf{K} , is:

$$\mathbf{K} = (\mathbf{J}^T)^{-1} \mathbf{K}_j (\mathbf{J})^{-1} \quad (16)$$

where \mathbf{J} is the robot arm analytical Jacobian matrix:

$$\mathbf{J} = \begin{bmatrix} -l_1 \sin(\theta_1) - l_2 \sin(\theta_1 + \theta_2) & -l_2 \sin(\theta_1 + \theta_2) \\ l_1 \cos(\theta_1) + l_2 \cos(\theta_1 + \theta_2) & l_2 \cos(\theta_1 + \theta_2) \end{bmatrix} \quad (17)$$

The compliance \mathbf{C} is the inverse of \mathbf{K} :

$$\mathbf{C} = \mathbf{K}^{-1} \quad (18)$$

From (14) and (18) emerges the role of biarticular actuator in stiffness/compliance modulation. Biarticular actuation can modulate the stiffness/compliance in both joints at the same time.

4. EXPERIMENTAL SETUP

A two-link planar robot arm with VSAs and two interchangeable actuation structures — the traditional monoarticular and human-like biarticular — is shown in Fig. 3. In both actuation structures, two VSAs are implemented. For the VSMA structure, one VSA is fixed on the arm base and connected to joint 1 via wires, and another is fixed on link 1 and connected to joint 2 via wires.

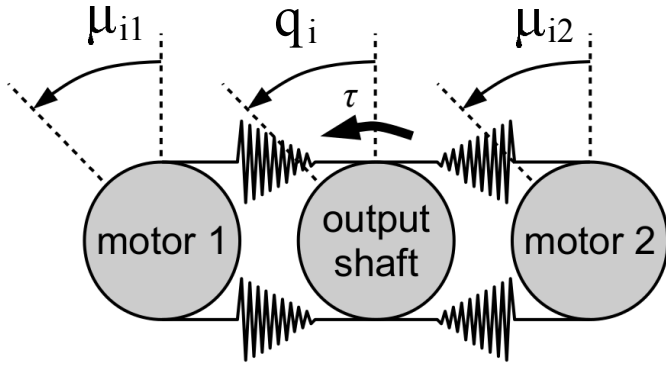


Fig. 4. Schematic of the VSAs QB Move Maker Pro

Table 1. Two-link arm parameters

$l_1 = l_2$	0.250 (m)
Pulleys radii $r_a = r_1 = r_2 = r_{12}$	0.0225 (m)
Actuators	QB Move Maker Pro (QB Robotics)

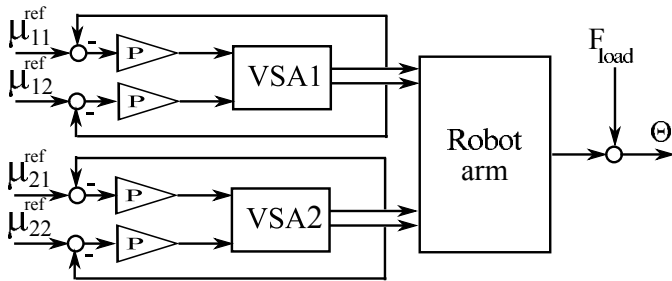


Fig. 5. Control scheme

A schematic of the VSA QB Move Maker Pro is shown in Fig. 4. The nominal output torque of the QB Move Maker Pro is:

$$\tau_i = 0.023 \sinh(6.733(q_i - \mu_{i1})) + 0.022 \sinh(6.960(q_i - \mu_{i2})) \quad (19)$$

where u_{i1} and u_{i2} for $i = (1, 2)$ are the antagonistic motor angles of actuator i , and q_i is the actuator i shaft angle. The QBmove nominal stiffness is:

$$\sigma_i = 0.155 \cosh(6.733(q_i - \mu_{i1})) + 0.153 \cosh(6.960(q_i - \mu_{i2})) \quad (20)$$

The compliance of the transmission system is considered to be negligible with respect to the compliance of the VSAs, therefore $q_i = \theta_i$.

The parameters of the two-link arm are shown in Tab. 1.

4.1 Analysis method

The VSMA and the VSBA structures are compared in terms of end effector compliance isotropy. Three robot arm initial positions are considered: $\theta = [-60, 120]^T$, $\theta = [-45, 90]^T$, and $\theta = [-30, 60]^T$. The robot arm is set in the initial position and then the motor positions (μ_{11} , μ_{12} , μ_{21} , μ_{22} in Fig. 4) are kept constant by position feedback control as shown in Fig. 5. A force (F_{load}) with constant magnitude of 1.08 N is applied at the end effector using a suspended weight with the force redirected in the horizontal plane using a pulley system. The direction of F_{load} is varied for $\theta_{load} \in (0, 360^\circ)$ every 0.25° . For every applied F_{load} the joint position at the equilibrium position is measured, and the end effector position is calculated. The

Table 2. Position reference values of the VSAs motors in the three arm positions

$\theta_1 (^\circ)$	$\theta_2 (^\circ)$	stiffness	$\mu_{11}^{ref} (^\circ)$	$\mu_{12}^{ref} (^\circ)$	$\mu_{21}^{ref} (^\circ)$	$\mu_{22}^{ref} (^\circ)$
-30	60	low	-31	-29	59	61
		high	-43	-17	47	73
-45	90	low	-46	-44	89	91
		high	-58	-32	77	103
-60	120	low	-61	-59	119	121
		high	-73	-57	107	133

Table 3. Condition number (cn) of end effector compliance

$\theta (^\circ)$	Actuator stiffness	Compliance condition number (cn)	
		VSMA	VSBA
[-30, 60] ^T	low	0.09	0.31
	high	0.08	0.34
[-45, 90] ^T	low	0.15	0.55
	high	0.13	0.58
[-60, 120] ^T	low	0.34	0.29
	high	0.27	0.31

end effector compliance for a certain end effector displacement direction θ_{dis} in the horizontal plane is defined as:

$$C_{\theta_{dis}} = \frac{\delta_{xy}}{|F_{load}|} \quad (21)$$

where δ_{xy} is the displacement magnitude between the end effector initial and equilibrium position.

As an index of isotropy for the end effector compliance the condition number (cn) is used. The condition number of Cartesian stiffness is defined as the ratio between the stiffness largest and smallest eigenvalues Kashiri et al. (2013). Considering that the compliance is the inverse of stiffness, the compliance condition number in this work is defined as:

$$cn = \frac{\min(C_{\theta_{dis} \in (0, 360^\circ)})}{\max(C_{\theta_{dis} \in (0, 360^\circ)})} \quad (22)$$

A high cn is desirable in order to have a homogeneous response of the compliance at the end effector in respect to the direction of applied forces.

Two actuator stiffness conditions are taken into account: low and high stiffness. For the case of low stiffness, the reference value of $\mu_{i1} = \theta_i^{des} - 1^\circ$ and $\mu_{i2} = \theta_i^{des} + 1^\circ$, for high stiffness the reference value are $\mu_{i1} = \theta_i^{des} - 13^\circ$ and $\mu_{i2} = \theta_i^{des} + 13^\circ$. In Tab. 2 the position reference values of the VSAs motors are listed with respect to the robot arm positions.

5. RESULTS

In Fig. 6 the resulting end effector displacements from the initial position for low and high actuator stiffness and for both the actuation structures and for the three arm position are shown. The displacements in Fig. 6 are used to calculate the end effector compliance using (21).

In Fig. 7 the end effector compliance with respect to the displacement direction for low and high actuator stiffness and for both the actuation structures are shown. The compliance of the VSMA structure shows higher values for both minimum and maximum compliance as the arm stretches toward a singular configuration. This results in a lower end effector isotropy as shown in Tab. 3.

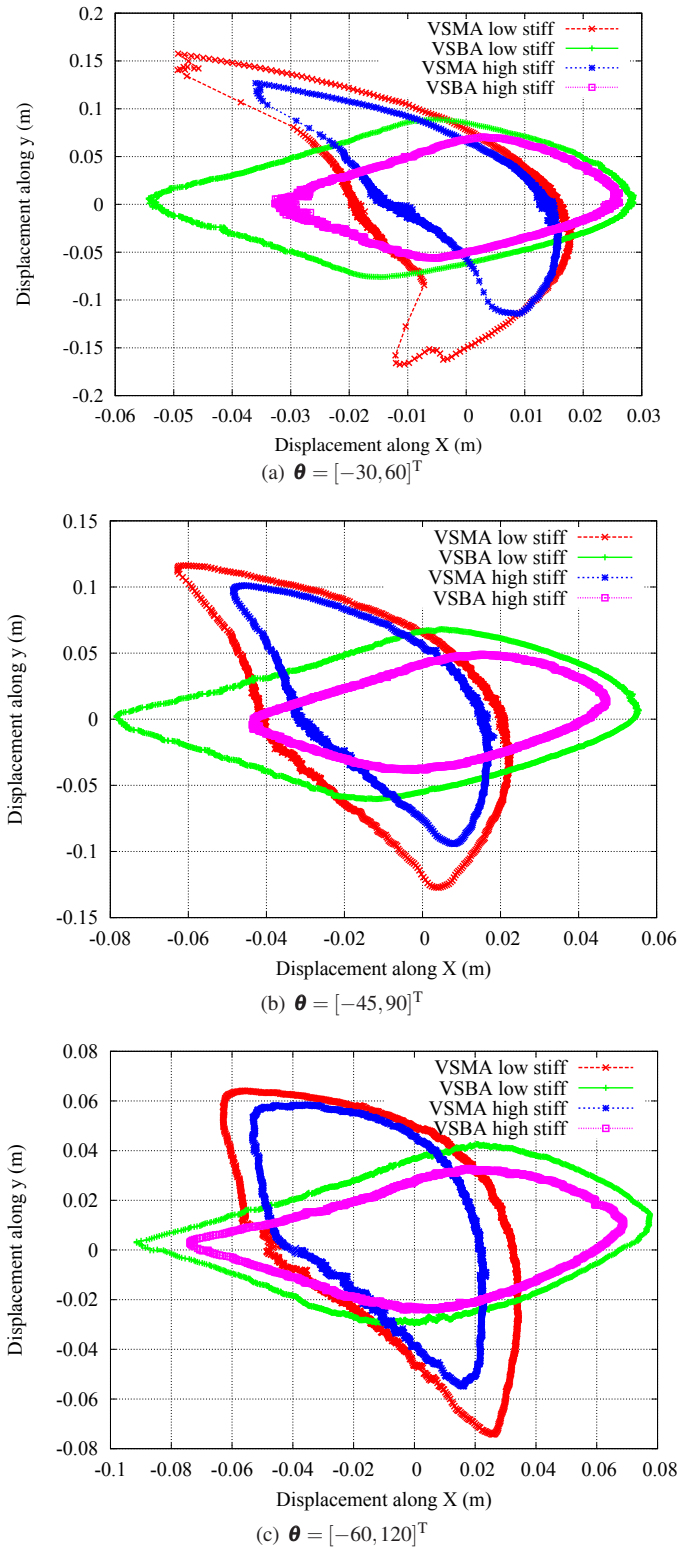


Fig. 6. Effector displacement from the initial position for low and high actuator stiffness and for VSMA and VSBA structures

6. CONCLUSIONS

End effector compliance isotropy is a key aspect for safety and performance of intrinsically compliant robot arms. In this work, we experimentally evaluate the end effector intrinsic

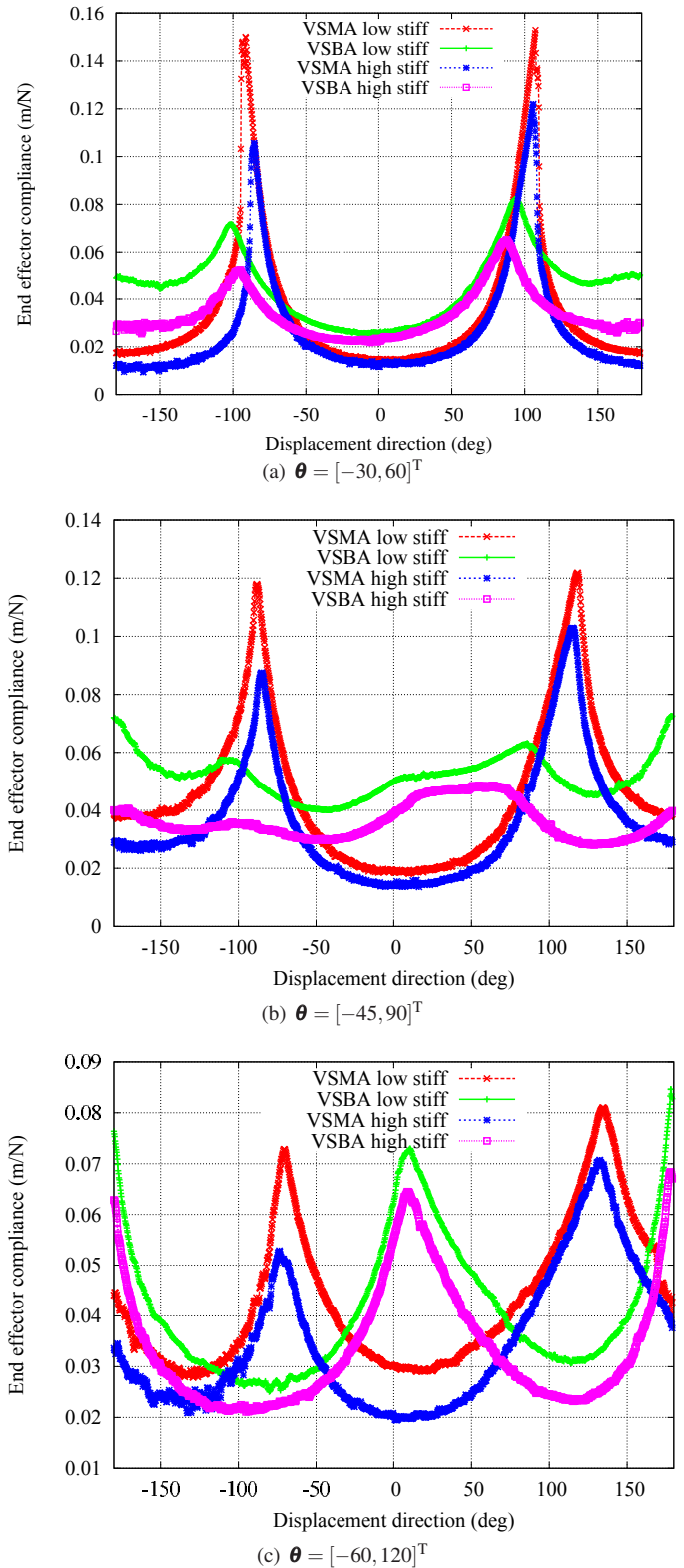


Fig. 7. End effector compliance for low and high actuator stiffness and for VSMA and VSBA structures

compliance isotropy of a two-link planar arm with Variable Stiffness Actuators (VSAs). The end effector intrinsic compliance is measured for two actuation structures, the traditional monoarticular and human-like biarticular. In comparison with the monoarticular VSA structure, the end effector compliance in the biarticular VSA structure shows a higher isotropy when

the arm extends towards singular configurations, which are challenging from a control point of view. As the isotropy of the end effector stiffness a key aspect in the design of intrinsically compliant manipulators, the pairing of VSAs and biarticular actuators better fits the requirements of intrinsically safe and high performance robot arm.

REFERENCES

- Bicchi, A., Rizzini, S., and Tonietti, G. (2001). Compliant design for intrinsic safety: general issues and preliminary design. In *2001 IEEE/RSJ International Conference on Intelligent Robots and Systems, 2001. Proceedings*, volume 4, 1864–1869.
- Chalon, M., Wimbock, T., and Hirzinger, G. (2010). Torque and workspace analysis for flexible tendon driven mechanisms. In *2010 IEEE International Conference on Robotics and Automation (ICRA)*, 1175–1181.
- Daley, M.A., Usherwood, J.R., Felix, G., and Biewener, A.A. (2006). Running over rough terrain: guinea fowl maintain dynamic stability despite a large unexpected change in substrate height. *J Exp Biol*, 209(1), 171–187.
- English, C. and Russell, D. (1999). Mechanics and stiffness limitations of a variable stiffness actuator for use in prosthetic limbs. *Mechanism and Machine Theory*, 34(1), 7–25.
- Fukusho, H., Sugimoto, T., and Koseki, T. (2010). Control of a straight line motion for a two-link robot arm using coordinate transform of bi-articular simultaneous drive. In *Advanced Motion Control, 2010 11th IEEE International Workshop on*, 786–791.
- Ham, R., Sugar, T., Vanderborght, B., Hollander, K., and Lefeber, D. (2009). Compliant actuator designs. *IEEE Robotics Automation Magazine*, 16(3), 81–94.
- Ham, R.V., Damme, M.V., Verrelst, B., Vanderborght, B., and Lefeber, D. (2007). MACCEPA, the mechanically adjustable compliance and controllable equilibrium position actuator: A 3DOF joint with two independent compliances. *International Applied Mechanics*, 43(4), 467–474.
- Hogan, N. (1985). Impedance control: An approach to manipulation: Part III—Applications. *Journal of Dynamic Systems, Measurement, and Control*, 107(1), 17–24.
- Horita, T., Komi, P.V., Nicol, C., and Kyrlinen, H. (2002). Interaction between pre-landing activities and stiffness regulation of the knee joint musculoskeletal system in the drop jump: implications to performance. *European Jour. of Appl. Physiology*, 88(1-2), 76–84.
- Hurst, J., Chestnutt, J., and Rizzi, A. (2010). The actuator with mechanically adjustable series compliance. *IEEE Transactions on Robotics*, 26(4), 597–606.
- Kashiri, N., Tzagarakis, N.G., Laffranchi, M., and Caldwell, D.G. (2013). On the stiffness design of intrinsic compliant manipulators. In *2013 IEEE/ASME International Conference on Advanced Intelligent Mechatronics (AIM)*, 1306–1311.
- Koganezawa, K., Inaba, T., and Nakazawa, T. (2006). Stiffness and angle control of antagonistically driven joint. In *The First IEEE/RAS-EMBS International Conference on Biomedical Robotics and Biomechanics, 2006. BioRob 2006*, 1007–1013.
- Kumamoto, M., Oshima, T., and Yamamoto, T. (1994). Control properties induced by the existence of antagonistic pairs of bi-articular muscles – mechanical engineering model analyses. *Human Movement Science*, 13(5), 611–634.
- Migliore, S., Brown, E., and DeWeerth, S. (2005). Biologically inspired joint stiffness control. In *Proceedings of the 2005 IEEE International Conference on Robotics and Automation, 2005. ICRA 2005*, 4508–4513.
- Oh, S., Kimura, Y., and Hori, Y. (2010). Reaction force control of robot manipulator based on biarticular muscle viscoelasticity control. In *Advanced Intelligent Mechatronics (AIM)*, 1105–1110.
- Oh, S., Salvucci, V., and Hori, Y. (2011). Development of simplified statics of robot manipulator and optimized muscle torque distribution based on the statics. In *American Control Conference (ACC)*, 4099–4104.
- Palli, G., Melchiorri, C., Wimbock, T., Grebenstein, M., and Hirzinger, G. (2007). Feedback linearization and simultaneous stiffness-position control of robots with antagonistic actuated joints. In *2007 IEEE International Conference on Robotics and Automation*, 4367–4372.
- Pratt, G. and Williamson, M. (1995). Series elastic actuators. In *1995 IEEE/RSJ International Conference on Intelligent Robots and Systems 95. 'Human Robot Interaction and Cooperative Robots', Proceedings*, volume 1, 399–406 vol.1.
- Salvucci, V., Kimura, Y., Oh, S., and Hori, Y. (2013a). Force maximization of biarticularly actuated manipulators using infinity norm. *IEEE/ASME Transactions on Mechatronics*, 18(3), 1080–1089.
- Salvucci, V., Kimura, Y., Oh, S., and Hori, Y. (2011a). BiWi: bi-articularly actuated and wire driven robot arm. In *IEEE International Conference on Mechatronics (ICM)*, 827–832.
- Salvucci, V., Kimura, Y., Oh, S., and Hori, Y. (2011b). Experimental verification of infinity norm approach for force maximization of manipulators driven by bi-articular actuators. In *American Control Conference (ACC)*.
- Salvucci, V., Kimura, Y., Oh, S., and Hori, Y. (2013b). Non-linear phase different control for precise output force of bi-articularly actuated manipulators. *Advanced Robotics*, 27(2), 109–120.
- Salvucci, V., Kimura, Y., Oh, S., Koseki, T., and Hori, Y. (2013c). Comparing approaches for actuator redundancy resolution in bi-articularly actuated robot arms. *Mechatronics, IEEE/ASME Transactions on*.
- Salvucci, V., Oh, S., Hori, Y., and Kimura, Y. (2011c). Disturbance rejection improvement in non-redundant robot arms using bi-articular actuators. In *Intern. Symp. on Industrial Electronics (ISIE)*, 2159–2164.
- Smeets, J.B. (1994). Bi-articular muscles and the accuracy of motor control. *Human Movement Science*, 13(5), 587–600.
- Tzagarakis, N.G., Laffranchi, M., Vanderborght, B., and Caldwell, D. (2009). A compact soft actuator unit for small scale human friendly robots. In *IEEE International Conference on Robotics and Automation, 2009. ICRA '09*, 4356–4362.
- Van Ingen Schenau, G.J. (1989). From rotation to translation: Constraints on multi-joint movements and the unique action of bi-articular muscles. *Human Movement Science*, 8(4), 301–337.
- Wolf, S. and Hirzinger, G. (2008). A new variable stiffness design: Matching requirements of the next robot generation. In *IEEE International Conference on Robotics and Automation, 2008. ICRA 2008*, 1741–1746.